ANNALS OF GEOPHYSICS, 67, 4, NH435, 2024; doi:10.4401/ag-9159
OPEN ACCESS

Near field tsunamis on volcanic islands: Blueprint for risk management using Stromboli as a test bed

Emmie M. Bonilauri[1], Andrew J. L. Harris*,[1], Matteo Cerminara[2], Giorgio Lacanna[3], Domenico Mangione[4], Raphaël Paris[1], Catherine Aaron[5], Tomaso Esposti Ongaro[2], Maurizio Ripepe[3]

(1) Université Clermont Auvergne, Laboratoire Magmas et Volcans, OPGC, IRD, CNRS, Clermont, France
(2) Istituto Nazionale di Geofisica e Vulcanologia (INGV), Sezione di Pisa, Italy
(3) Università di Firenze, Dipartimento di Scienze della Terra, Firenze, Italy
(4) Dipartimento della Protezione Civile, Rome, Italy
(5) Université Clermont Auvergne, Laboratoire de Mathématiques Blaise Pascal, CNRS, Ferrand, France

Article history: received September 17, 2024; accepted October 03, 2024

Abstract

At Stromboli, coastline populations are exposed to near-field tsunami generated by flank collapses. Landslides on the Sciara del Fuoco can generate waves arriving in the village in less than a few minutes. Due to the hazard posed on Stromboli by tsunami, we have focused our research on answering three key questions in terms of mitigation: (1) How can a tsunami be detected and characterized in real-time? (2) What will be the likely event scenario and on-island impact of the resulting tsunami? (3) When and where will the tsunami arrive, and what is the evacuation capacity? To this end, we have convolved a method to assess escape times from tsunami-exposed coastal areas, with wave travel times and inundation assessments output from numerical simulations. Here we review the local situation in terms of hazard, risk and mitigation measures, and assess progress to date in preparing for tsunami on Stromboli to explore a blueprint for management actions at any near-field tsunami-exposed community.

Keywords: Island Volcano; Stromboli; Tsunami; Mitigation; Evacuation Time

1. Introduction

Whether active or inactive, volcanic islands and their unstable flanks are well known as sources of tsunamis (Paris, 2015; Paris et al., 2014a). The problem generally rests on the fact that volcanic islands are un-buttressed piles of poorly consolidated pyroclastic deposits, lavas and volcanoclastic breccia, all sitting on a highly deformable basement of sea floor sediments (Denlinger and Morgan, 2014). When such a pile has a subaerial height of 1-3 km, and a sub-marine depth of 2-4 km, the mass is unstable and capable of sector collapse to produce tsunamis of, locally, 10s of meters in height.

Although now subject to extreme doubt (see footnotes), literature of the 1980s through 2000s debated the potential of "giant" (100's km^3, Normark et al., 1993) collapses of Hawaiian island volcanoes for creating "megatsunami"

(McMurtry et al., 2004), and how such collapses may[1] be linked to tsunami deposits found at, for example, elevations of ~70 m above current sea level and 2 km inland on the Hawaiian island of Molokai (Moore, 2000). In addition, modelling of potential sector collapses of the Canary Islands were argued to have the potential[2] for tsunami impact along the eastern seaboard of the USA (Ward and Day, 2001; Tehranirad et al., 2015). Likewise, large volume (12 km^3) collapses of Etna's un-buttressed eastern flank (Calvari and Groppelli, 1996) were linked with rapid abandonment of villages along the Israeli coast ~8 ka, supposedly due to the tsunami thereby triggered (Pareschi et al., 2007). Etna's 7.59 ± 0.13 ka collapse events (Calvari and Groppelli, 1996) were also modelled as capable of generating waves of up to 1-5 m high along the coastlines of Tunisia, Libya and Egypt (Pareschi et al., 2007). Major explosive eruptions at volcanic islands are also well known tsunami triggers, the 1883 caldera-forming eruption of Krakatoa being the classic example (Paris et al., 2014b; Simkin and Fiske, 1983). In addition, "atmospheric forcing" (Schindelé et al., 2024) can occur during a high energy explosive eruption when pressure waves propagate into the atmosphere, with the tsunami being triggered from the interaction of the pressure waves with the ocean surface. This can have a global impact as witnessed during the 2022 eruption of Hunga Tonga (Lynett et al., 2022; Chacón-Barrantes et al., 2023).

However, here we focus on a more frequent hazard presented by lesser-scale collapses such as those witnessed at Anak Krakatau in 2018, Iliwerung (Lembata) in 1979, and on Paluweh Island in 1928 (Grilli et al., 2019; Mutaqin et al., 2019). Such collapses involve small volume (106-109 m^3) avalanches of volcanic material from the subaerial and/or submarine flanks (see Schindelé et al., 2024 for review), and/or collapse of lava flow fronts and/or lava ocean entry benches. In this latter regard, ocean-entry flows are known to form platforms underlain by breccia liable to sudden collapse (cf. Mattox and Mangan, 1997), and lava flows descending the steep seaboard flanks of volcanic islands have been observed to be inherently unstable, suffering near-constant flow front collapse (cf. Lodato et al., 2007). In all cases, the tsunami hazard needs to be mitigated for; but the problem is that: (i) there will be large and exposed shore line populations at risk, (ii) there will likely be little time between triggering event and wave impact at proximal (even distal) locations, so that there is little time for warning and evacuation of exposed populations, and (iii) there may be little, or no, robust historical or observational/geophysical data on which to base hazard scenarios, so that triggering and/or source conditions become a major cause of debate and uncertainty (cf. footnotes).

We here focus on the problem of preparing for and managing the volcanogenic tsunami hazard when faced with scenarios based on well-documented and observed events, such as the landslide tsunamis at Anak Krakatau in 2018 (Grilli et al., 2019; Paris et al., 2020) and Stromboli in 2002 (Tinti et al., 2006a; Fornaciai et al., 2019). Fundamentally, such events need to be, and can be, prepared for and are thus "manageable" in a human sense. On the volcano island source itself, the problem is most acute as, given that the source of the tsunami is on-island, and on an island that is just likely a few kilometers across, there will be very little time (minutes) between tsunami trigger and arrival. Then, given the proximity of the exposed population to the source (a few km), the tsunami will have a run up that is at its maximum on the source-island. There is also little time, just minutes (Tinti et al., 2006a), for the exposed population to be warned of, or to react to, the ingress of the tsunami.

Following the landslide-triggered tsunami of December 2002 on Stromboli (Aeolian Islands, Italy; Fig. 1), the island has become a focus of attention in preparing for tsunami impact on exposed population. Tsunami worst-case scenarios at Stromboli have envisaged a total collapse of the Sciara del Fuoco, where the ~5 ka collapse involved a volume of material of 0.97-1.81 km^3 (Kokelaar and Romagnoli, 1995) and the resulting tsunami has been modelled to have had a run up of 50 m (Tinti et al., 2000). Trenches dug on Stromboli at 3.5-4.2 m above current sea level have revealed three medieval tsunami deposits, intercalated with volcaniclastic deposits and primary tephra, showing evidence for tsunami following paroxysmal explosions and flank collapses, thus making Stromboli an island volcano "*particularly susceptible to tsunami generation*" (Pistolesi et al., 2020). Historical tsunamis with an on-island source,

1 We here place "may" in italics and use the Molokai example here, as doubt has been cast on whether the deposits found at 170 and 190 m above current sea level on Lanai by Stearns (1938) can be related to what Helsley and Helsley (2012) term the "Giant Wave Hypothesis". Instead Helsley and Helsley (2012), give evidence that the Lanai deposits are "uplifted strandlines formed during island uplift and glacial eustatic sea level variations." However, tsunami modelling of giant Hawaiian landslides from the Big Island of Hawaii by Johnson and Mader (1994) can support deposits found 25-60 m above current sea level (see also Felton et al., 2000, among others, for further discussion).

2 A problem with the mega-tsunami theory is that it rests on the assumption of a catastrophic and instantaneous failure of an island-volcano flank, when slumping is more likely continuous, piecemeal and gradual over time (e.g., Smith et al., 2002). As a result, for example, Pararas-Carayannis (2002) argues "a collapse of Cumbre Vieja will not generate waves of up to 50 m in height in Florida and the Caribbean islands". All the same, modelling by Mader (2001) of a "*plausible*" (Pararas-Carayannis, 2002) flank failure of La Palma provides far-field wave estimates of 3 m for the east coast of the USA and the Caribbean, and 10 m for European and African coasts.

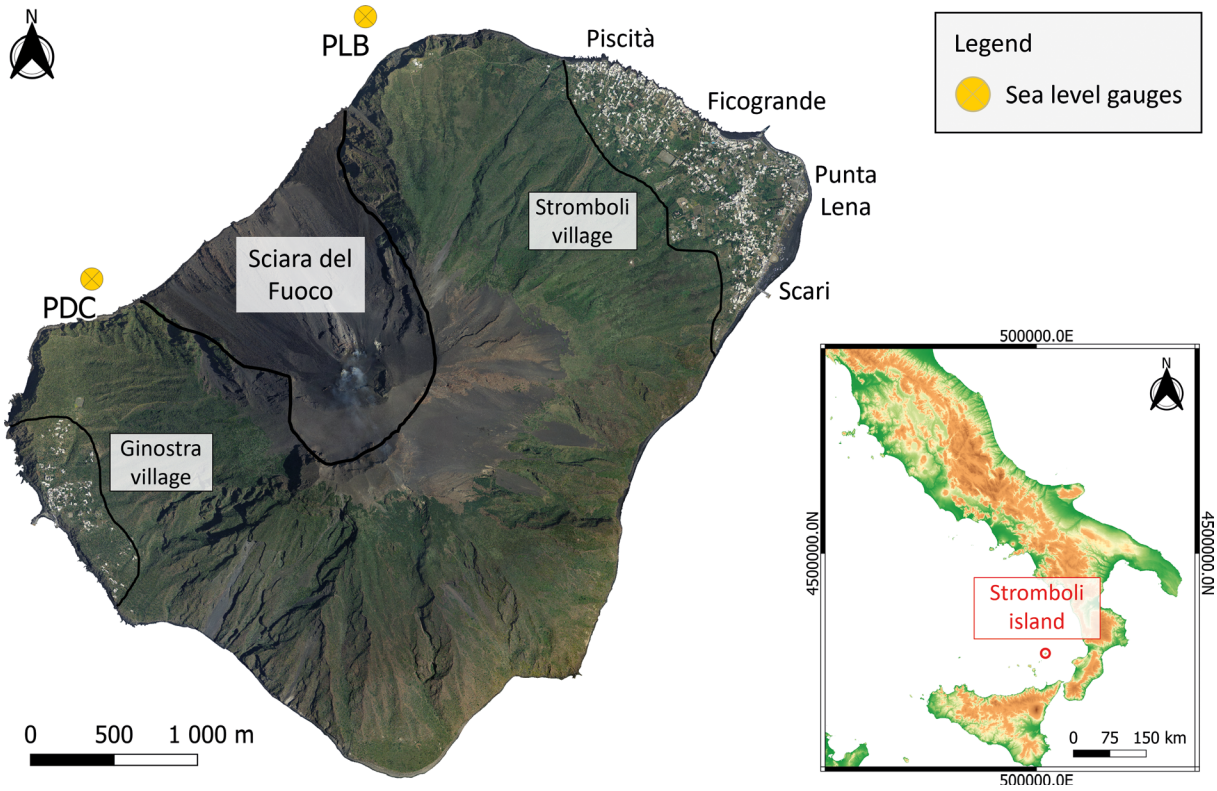

Figure 1. Location map for Stromboli with all on-island sites mentioned in the text and the locations of the sea level gauges marked.

either caused by landslides or pyroclastic flows entering the sea have been recorded as occurring in 1916, 1919, 1930, 1944, 1954, and 1988 (Maramai et al., 2005). These events, though, lack data, although the 1930 tsunami is known to have had a runup of 2-3 m (Roberto et al., 2014). There is also evidence that flank collapses of Stromboli between 1300 and 1400 AD, and involving ~10^9 m^3 of material, resulted in damage and casualties around the Gulf of Naples, 230 km from Stromboli (Rosi et al., 2019).

Due to the hazard posed by Stromboli as a volcano-island tsunami source, as well as the near-to-far field exposure (Fig. 2), Stromboli has become a focus of research into answering three key questions in terms of preparation:

(i) How can a tsunami be detected, recorded and characterized in real-time using near-source sea-floor pressure sensors (Schindelé et al., 2024; Ripepe and Lacanna, 2024);

(ii) What will be the likely event scenario and on-island impact of the resulting tsunami, a question answered using either information from historical records (Maramai et al., 2005), deposits (Pistolesi et al., 2020), and/or modelling (Esposti Ongaro et al., 2021);

(iii) When and where will the tsunami arrive, and what is the evacuation capacity (Bonilauri et al., 2021).

To this end, and following up on an collaboration between the Laboratoire Magmas et Volcans (LMV, Université Clermont Auvergne, France), the Laboratorio Geofisica Sperimentale (LGS, Università di Firenze, Italy), and the Istituto Nazionale di Geofisica e Vulcanologia (INGV, Pisa, Italy), within the framework of the DPC-INGV 2022-2024 agreement (DPC: Dipartimento della Protezione Civile, Roma, Italy), a collaboration has been federated under a project to carry out "*evacuation modeling and to convolve physical modeling of a tsunami with evacuation modeling*". This initiative, as funded by DPC for the period 2023-2025, has built on our initial efforts to assess escape times from tsunami-exposed coastal areas, as defined by the 10.9 m run up of the December 2002 tsunami, and a 4 minute escape time (Bonilauri et al., 2021), and brought in wave modelling to consider a variety of potential scenarios (Esposti Ongaro et al., 2021; Cerminara et al., 2024). We here review our progress to date in preparing for the Stromboli scenario, so as to explore a blueprint for management actions at any near-source tsunami-exposed community. After reviewing the local situation in terms of hazard, risk and management measures, we complete a synopsis of on-going research-led efforts to define the three main items that responding agencies, and the hazard manager, need. These being: *what, when and where*?

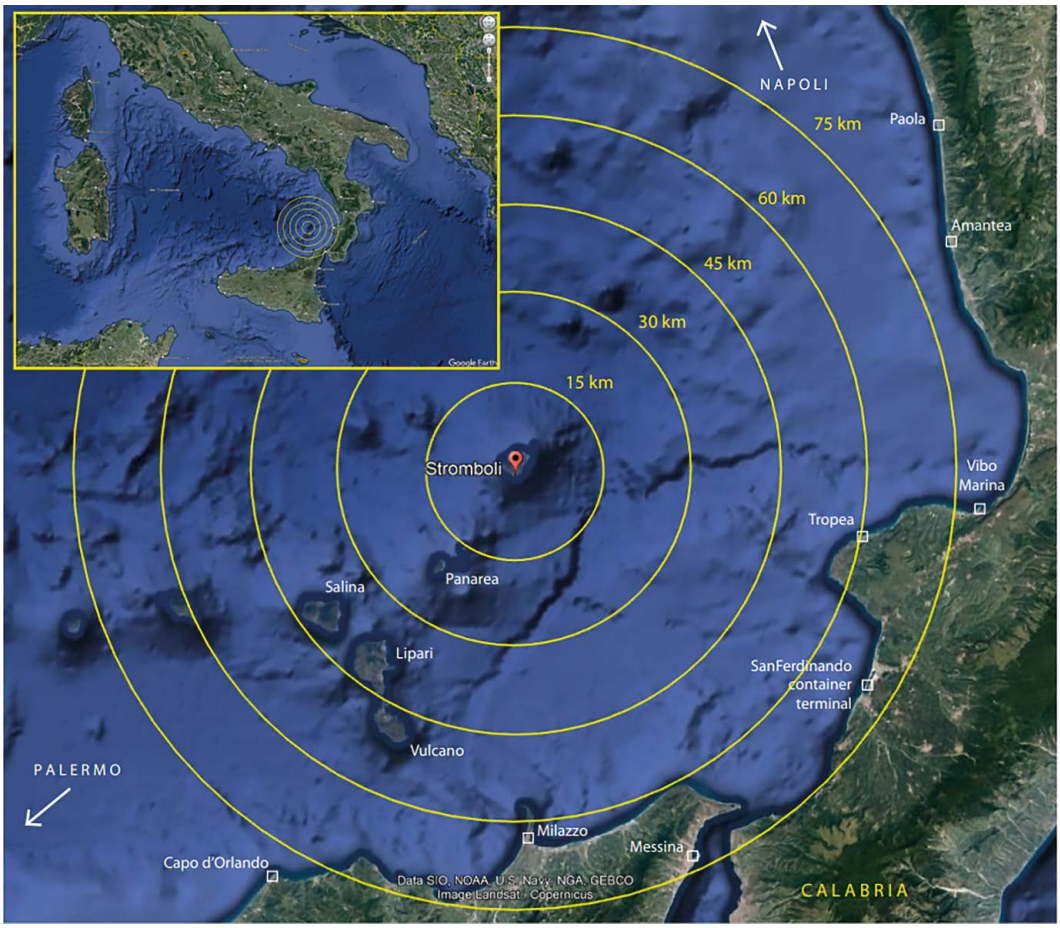

Figure 2. Radial distance from the summit of Stromboli to the main tsunami-exposed sites along the coasts of Calabria and Sicily, as well as other Aeolian islands.

2. Background

On December 30, 2002, two landslides occurred on the Sciara del Fuoco, at 13:15 (hh:mm, all times in this section are Central European Time, UTC+2) and the second at 13:22. While the first landslide was submarine with an estimated volume of 20×10^6 m^3 (Chiocci etal., 2008), the second was a sub-aerial landslide involving $4\text{-}9 \times 10^6$ m^3 (Tinti et al., 2006a). The second landslide was accompanied by fine wet ash (generated by rock collisions during the landslide) that fell on Stromboli's SE flank. The two landslides triggered two sets of tsunami, separated by 7 minutes that impacted the entire coastline of Stromboli in less than 4 minutes (Tinti et al., 2006a), with a run-up of 10.9 m (Tinti et al., 2006b). The waves moved faster in deeper water, reaching the island of Panarea, 20 km SW of Stromboli, in < 5 minutes (Tinti et al., 2006a), with impacts being recorded as far as Milazzo in Sicily (Fig. 2), where an oil tanker encountered difficulties. Damage was recorded at all sea-level locations along the coast at Stromboli village between the Piscità and Scari (Fig. 1), but only six people were evacuated by helicopter and taken to two hospitals in Sicily due to the extremely low shoreline population density during the winter.

A survey made by us in January 2020 showed there to be just six permanently occupied units in the 2002 run-up zone, with all being located at Punta Lena (Fig. 1). All other units within the 2002 run-up zone, within which we identified 123 exposed buildings, were hotels, vacation rentals, seasonal beach-side bars-restaurants-shops, and/or summer residences, all of which were boarded-up for winter at the time of the survey. Interviews made as part of the same survey revealed that residents knew they were in a high risk zone but had no means to move out of it. In fact, the coastal area was recognized has having been used prior to the 1950s only as a warehouse and boathouse zone, where fishermen lived higher in the village and commuted down to the beach during the day as the coastal zone was known to be a dangerous place in terms of tsunami hazard, and so not a good place to spend the night asleep. Further, interviewees recalled that the sound of rolling boulders being carried out to sea by rapidly retreating water

was the sign of danger, i.e., the tsunami was on its way; and so, evacuation should be immediate upon hearing such a sound. This is a memory for many populations in tsunami-exposed areas (e.g., Carvajal et al., 2019; Dudley, 1998; Eaton et al., 1961; Klettner et al., 2012), where it is well known that "*the sea abruptly retreats, sometimes for many 100 m and usually several minutes before the arrival of the first wave crest, depending on the wave period*" (Röbke and Vött, 2017)[3]. Exposure is thus highest during the summer months when all sea front properties are open and occupied, night and day, by tourists with no such memory, and when there is high volume of day-tipper traffic visiting on tour boats from Calabria (Tropea), Sicily (Messina and Milazzo), and other Aeolian islands (Fig. 3a).

Figure 3.(a) Simultaneous arrival of four day trip boats and the aliscafo (hydrofoil) from Milazzo-Lipari (combined capacity ~1500 passengers). A commercial fishing boat is also tied up, and there is on-going construction work (see JCB in the background). Photo taken around 17:30 on 18 June 2024. (b) Signs installed in 2011 and updated in July 2024 to warn of tsunami hazard at the highly exposed location of Punta Lena (left) and gathering points for the scuola (school) zone in the case of an emergency (right).

The potential for loss led to efforts from 2003 onwards to (i) increase awareness of the hazard, and (ii) allow detection and provide early warning. In terms of awareness, signage was put in place (Fig. 3b), and a National civil protection presence (Bertolaso et al., 2009) was maintained on the island until 2013, when under Italian law the government-mandated period of "national emergency" ended and hazard management duties were passed back to the Mayor of Lipari. For early warning, beginning in 2007, LGS began to design, build and install a sea-floor pressure sensor capable of detecting, and alerting to tsunami waves (Fig. 4a). The detection system involves two pressure sensors (produced by Idromar International, San Giuliano Milanese, Italy) installed on an elastic beacon at depths of 14 and 48 m below the sea surface. Outputs from both sensors are sampled at 125 Hz, de-spiked and low-pass filtered below 15 s (Ripepe and Lacana, 2024). The depth of the pressure sensor on the seabed (48 m) is optimal for reduction of noise from sea waves at a period of 13 s, thus guaranteeing the best signal-to-noise ratio in the wave range (50-120 s) typical of tsunami-generated by landslides. Two beacons were subsequently installed offshore of the Sciara del Fuoco (Fig. 4b): at Punta dei Corvi (PDC) in 2008 and Punta Labronzo (PLB) in 2017 (Fig. 1). A tsunami

3 However, sea retreat prior to a tsunami is far from being systematic. During meetings with exposed populations, this is something that we remind the population: do not expect the sea to retreat each time a tsunami comes. It can be a last-minute warning sign, but it depends on the tsunami source geometry and near-shore bathymetry.

early-warning algorithm was then developed to run in real-time, allowing alert within a minute of onset of the trigger event and 10 seconds before capture of the maximum wave height (Ripepe and Lacanna, 2024). Given a 4 minute arrival time for the tsunami *every second counts*, so there is no time to process the full (2-3 minutes long) signal (Fig. 4c). Note that, this algorithm is frequency based, and work is ongoing to insert into the early warning system information also based on the wave amplitude. On July 3 and August 28, 2019, two tsunamis were triggered by entry of pyroclastic flows into the sea at the Sciara del Fuoco (Giordano and De Astis, 2021). The tsunami of July 3 was detected just 7 seconds (at PDC) and 16 seconds (at PLB) after the triggering event, i.e., entry of the pyroclastic flow into the sea (Fig. 4c). In August 2019, the tsunami was automatically detected 11 seconds following the triggering

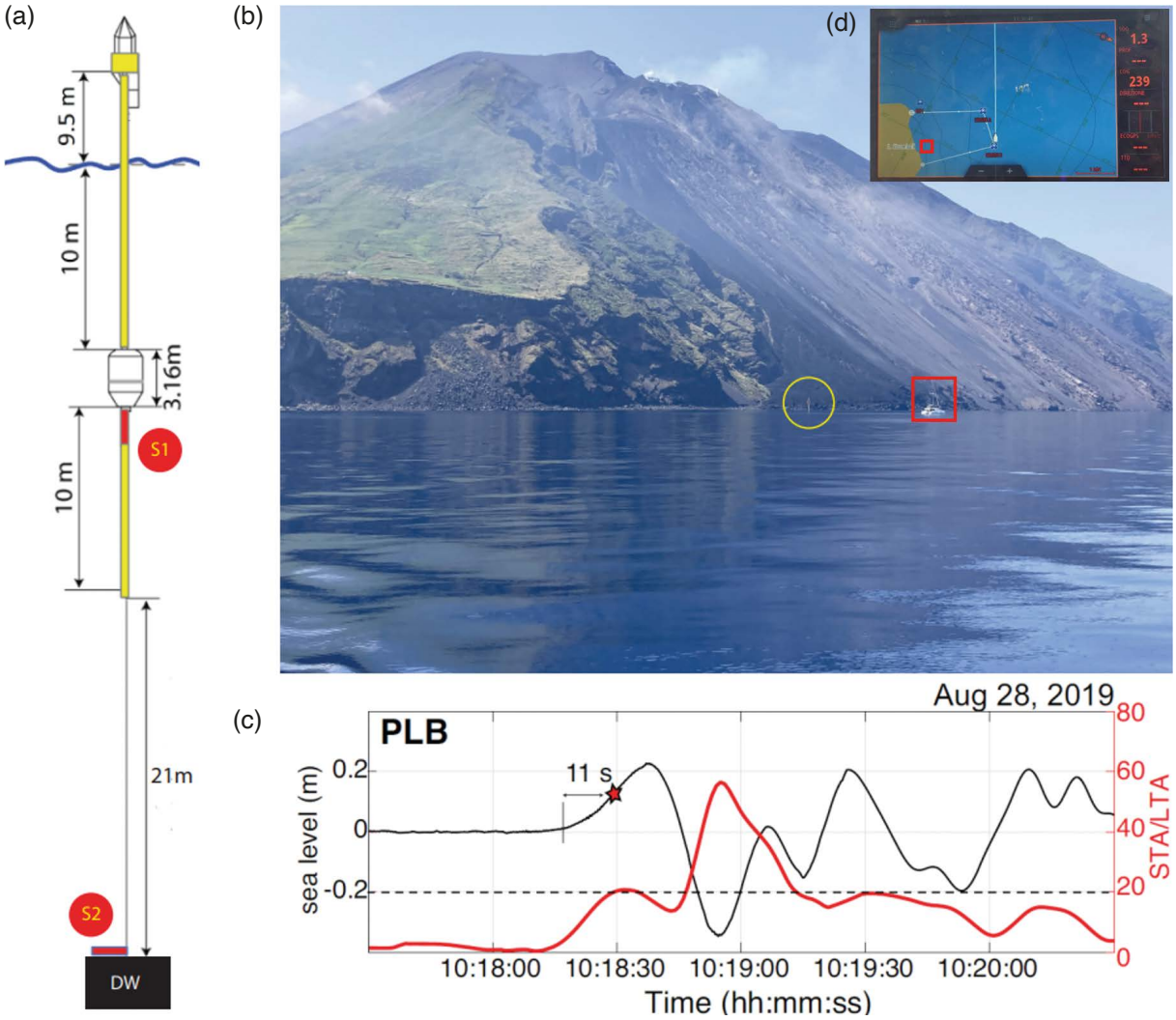

Figure 4. (a) Design of elastic beacon (modified from Schindelé et al., 2024) where S1 is the pressure sensor at 14 m depth, and S2 that at 48 m depth, i.e., on the sea floor. DW is the dead weight that anchors the system to the sea floor. (b) Photo of the PDC station with the foot of Sciara del Fuoco in the background, where yellow circle highlights the above sea surface portion of the system responsible for transmission. Note the yacht to right of beacon and in front of the Sciara del Fuoco. (c) Waveform recorded by the PLB sensor during passage of the tsunami triggered by entry of the August 28, 2019, pyroclastic flow into the sea. Black trace gives the sea level change, red the STA/LTA[4] ratio. The star indicates when STA/LTA is above threshold (dashed line), at which point the tsunami warning is triggered (after Ripepe and Lacanna, 2024). (d) GPS monitor showing exclusion zone in front of Sciara del Fuoco (white trapezoid), the location of the boat (craft symbol) and the boat trajectory (blue line). Red box gives the location of the yacht pictured in (b).

4 Following Allen (1978), the detection algorithm is based on real-time analysis of the waveform in terms of the short-term average (STA) and long-term average (LTA) average ratio. When STA/LTA ≥ 20, an alert is triggered (Ripepe and Lacanna, 2024).

event, an event that had a positive amplitude of only 0.2 m, thus indicating the high sensitivity of the detection system (Ripepe and Lacanna, 2024). Starting from October 2019, upon detection sirens deployed on Stromboli and Panarea are automatically activated, within the framework of an experimental early-warning system. In addition, there is an acoustic alarm located in the operational room of the Coast Guard in Milazzo.

Based on these time-lines (i.e., a warning-to-wave arrival time of 4 minutes), in Bonilauri et al. (2021) we developed a model to assess the evacuation capacity of the impact zone, this being a flooded zone defined by DPC as based on the measured run up of the 2002 tsunamis (Tinti et al., 2006a). The approach of Bonilauri et al. (2021) involves mapping all exposed buildings and their exit points (aka Doors of Exposed Buildings, DEB), linking these to impact area escape points (Refuge Area Entry Points, RAEP), and assessing the time needed to travel (on foot) between each DEB and RAEP. Escape speed was assessed on the basis of street width and slope, and DEB were coded green if the escape time was less than 4 minutes, and red if not (Fig. 5a). Across the red zone, 123 buildings were identified with a total of 534 doors, for an average of around four DEB per building. We quantized the zone in terms of 316 escape centroid starting points, of which 104 were green. We further developed DEB-tailored evacuation maps for each door in the red zone, giving the escapee the quickest possible evacuation route (Fig. 5b). To conform to standard, these maps were designed in the style of standard building escape maps in the case of fire, and/or evacuation of planes and/or ships in the case of incident (Bonilauri et al., 2021).

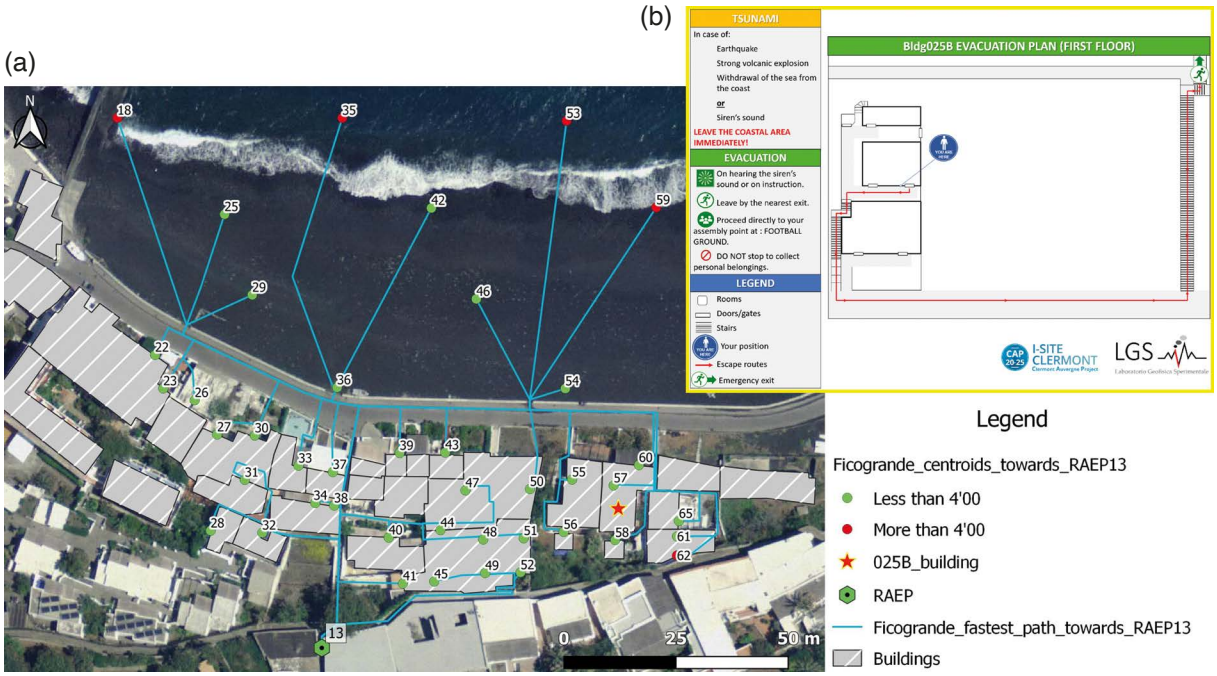

Figure 5. (a) Central sector of Ficogrande for whom escape via RAEP13 is the quickest option. The fastest escape routes from each centroid (18 through 65) are marked with blue lines. All but the centroids in the sea, plus centroid 62, are green meaning 44 points are inside the 4 minute wave arrival threshold (from Bonilauri et al., 2021). (b) Evacuation plan for building 025B (from Bonilauri et al., 2021).

In terms of mitigation the fundamental problem is lack of data. For example, at Stromboli the run up zone for hazard assessment is based on field observations and eyewitness interviews just after the December 2002 tsunami (Maramai et al., 2005; Tinti et al., 2006b). However, field mapping is difficult given the subtle and ephemeral nature of tsunami traces (driftwood, sedimentary deposits, etc.), so that we found the inundation zone defined for December 2002 to be too conservative. For example, in Bonilauri et al. (2021) we interviewed householders who described finding flooded basements and cellars (upon returning to their residence after the initial interview survey in January and March 2003), in spite of being 100 m inland of the inundation zone assigned to Punta Lena. In addition, the spatial distribution of the deposits will not correspond exactly to the spatial distribution of the inundation. Indeed, the fine-grained deposits left at the limit of inundation are not preserved for very long. Surveys based on historical records can also be made, but historical records lack rigor in terms of completeness of coverage and quantification.

For example, reliable values for tsunami run up at all exposed locations will almost certainly not be available. Tsunami deposit analyses can provide useful constraint, but still may only involve two or three events and locations, with uncertain relations between the source (landslide volume and location) and impact (on-land flooding depth at all exposed locations), thus preventing statistical and/or probabilistic analyses. We have thus been working on a model-driven protocol, where wave properties (mostly travel time to exposed point plus extent and depth of flooding at all on-land locations), is driven through multiple runs of a tsunami propagation model, as validated to the case in hand. For Stromboli, we thus use the output from multiple simulations using Multilayer-HySEA (Fernández-Nieto et al., 2018; Macías et al., 2021a,b; Cerminara et al., 2024), as validated through best-fit to the 2002 tsunami (Fornaciai et al., 2019; Esposti Ongaro et al., 2021). We then convolve the output of Multilayer-HySEA with our escape model to produce best escape time and route scenarios for the full range of plausible events and source term combinations (Bonilauri et al., 2024). We herein describe this convolution.

3. Methodology

Our method involves exploiting simulation results of Multilayer-HySEA runs from 11 subaerial and submarine positions, for five volumes between 5 and 30 × 10^6 m^3, and three different landslide densities (Fig. 6). This data set of 198 simulations is given in https://doi.org/10.13127/stromboli/sciara_del_fuoco_tsunami (Cerminara et al., 2024). For each combination of position, volume and density, the key source terms are the flooded zone and wave travel time to all points flooded in each tsunami scenario. For our assessments, we use a grid cell size of 20 m this being defined by the resolution of Multilayer-HySEA and the digital elevation model that we use (Bonilauri et al., 2024). Then, from the centroid of each inundated grid cell we project the fastest route to the edge of the flooded zone, this being the RAEP. For details on modelling pedestrian escape time see Bonilauri et al. (2021).

If the time to reach the RAEP (t_{RAEP}) is greater than the wave travel time (t_{wave}) to any given cell, then the point is outside of the threshold time ($t_{threshold}$) and the centroid is color coded red. Instead, if the time to reach the RAEP is less than the wave travel time to any given cell, then the centroid is color coded green (i.e, $t_{RAEP} < t_{wave}$). Finally, we produce synthetic waveforms for the pressure sensor at PDC (Fig. 4) and, using a statistical analysis (the LASSO approach of Tibshirani, 1996), of the pressure sensor waveform. We link the waveform with potential inundated area upon receipt of 40 seconds of sensor data. For full details see Bonilauri et al. (2024).

4. Results

We present the results in terms of answering the three key questions that a hazard management system needs, i.e., what, when and where? Specifically, we need to know:

- What is the height of the wave and its variation with distance?
- When will the wave arrive at the sensor and the coastline?
- Where will flooding occur?

This "*what, when and where*" information then allows us to project the most efficient escape routes from each exposed cell, and assess the threat posed to each cell in terms of escapability (i.e., IF $t_{RAEP} < t_{wave}$ then green; ELSE red, meaning that the point is defined as being *outside* of $t_{threshold}$, the former condition being *inside* $t_{threshold}$).

4.1 What: Modelling the wave

Maximum wave height increases with landslide volume, where at-source wave heights increase from 5-10 m for a volume of 5 × 10^6 m^3, to 25-40 m for a volume of 30 × 10^6 m^3 (Fig. 7). These values are for subaerial positions, but as we move to submarine positions, wave height decreases to the extent that a 5 × 10^6 m^3 landslide at a depth of −511 m below sea level (position 9, Fig. 6) has a negligible effect. Wave heights diminish around the island, with the largest waves being directly in front of the Sciara del Fuoco as well as around the western and eastern shorelines. This has implications for offshore craft (note, in Fig. 4d, the position of the yacht inside the exclusion zone that extends 2 nautical miles from the foot of the Sciara del Fuoco).

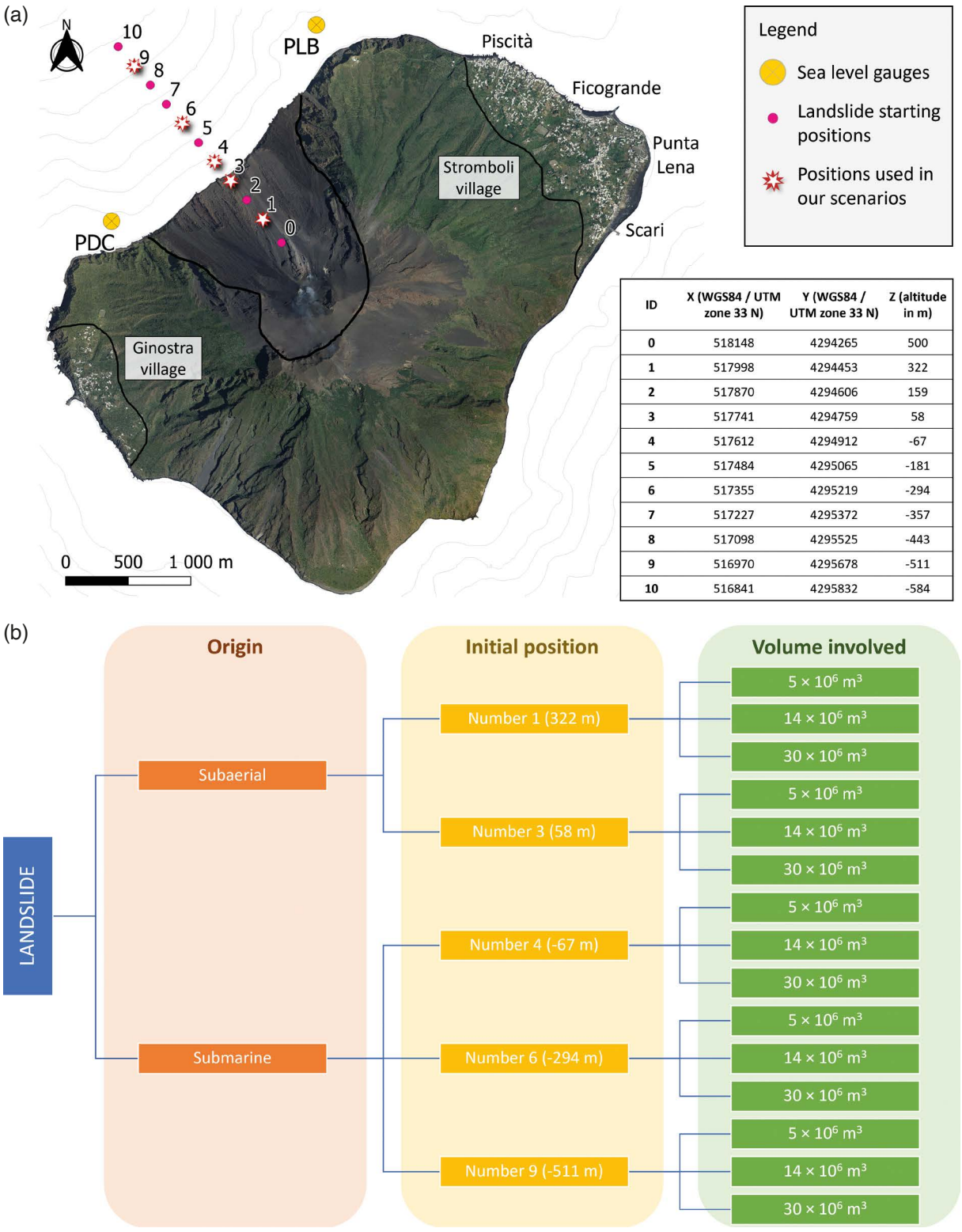

ID	X (WGS84 / UTM zone 33 N)	Y (WGS84 / UTM zone 33 N)	Z (altitude in m)
0	518148	4294265	500
1	517998	4294453	322
2	517870	4294606	159
3	517741	4294759	58
4	517612	4294912	-67
5	517484	4295065	-181
6	517355	4295219	-294
7	517227	4295372	-357
8	517098	4295525	-443
9	516970	4295678	-511
10	516841	4295832	-584

Figure 6. (a) The 11 landslide-triggered tsunami generation scenarios used by Bonilauri et al. (2024). These are the red dots labelled 0 through 10 and as tabulated. For purposes of demonstration, in this review we only consider two subaerial positions and three submarine positions (stars). (b) The model run tree giving the position and volume of each tsunami scenario considered here.

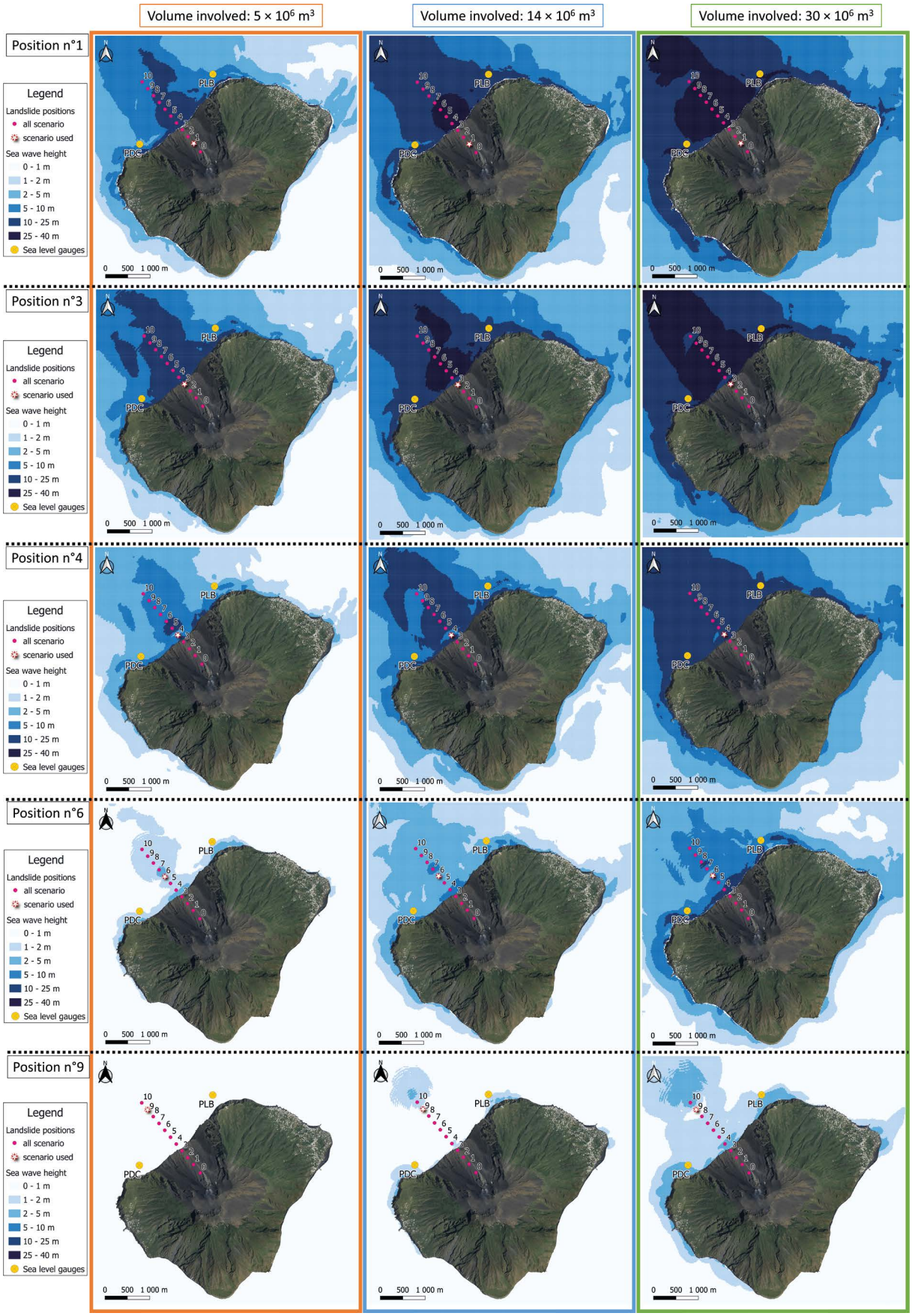

Figure 7. Spatial distribution of tsunami wave height for three landslide volumes and five positions (see text for explanation).

4.2 When: Alerting for wave arrival

Larger volumes produce higher waves that move at greater speed. Thus, a wave generated by a 30×10^6 m^3 wave will be detected 10 seconds before a wave from a 5×10^6 m^3 landslide (Fig. 8 and Fig. 9). Given that the detector algorithm automatically triggers the sirens after 4 seconds, this means that theoretically the sirens alert to the larger landslide 24 seconds after it begins, and 34 seconds after slip onset for the smaller landslide. For subaerial landslides, with each increase in volume the amplitude of the wave approximately doubles. Instead, the time between the arrival of the first and second waves at the sensor remains roughly the same at about 60 seconds, the time being a little shorter for smaller volumes. For deep submarine landslides the first wave is much less pronounced (< 1 m) than the second wave (2-7 m, depending on position), and the time between the two waves reduces to < 40 seconds. Even if differences are only a few seconds to a few tens of seconds, when an exposed population has only a few minutes to react, any extra time available is precious. Note, also in the case of deep submarine position 9 (Fig. 6), the first wave is negligible, and it is the second that needs to be mitigated for, again adding nearly a minute to the time available.

In terms of tsunami arrival time, the SW and NE coasts are affected in less than 2 minutes, depending on the scenario. For the same location, the greater the volume of the landslide, the faster the tsunami will reach the coast. In all scenarios, the Piscità district (Fig. 1) is the most exposed, with tsunami arrival times between 60 and 180 seconds. The arrival time increases towards the East, with the Scari district (Fig. 1) being the flooded between 180 and 600 seconds after landslide onset.

4.3 Where: Assessing the spatial distribution of impact

In terms of inundation, the NE coast, the narrow beach zone along the SE coast, and the southern point of Stromboli are the most exposed locations (Fig. 10). At Punta Lena, for a tsunami triggered by a 30×10^6 m^3 subaerial landslide, flooding to depths of up to 15 m can extend 500 m inland where the near-coast topography is relatively flat. Elsewhere, such as between Piscità and Ficogrande where buildings are located on 10 m high sea cliffs, and at Scari where the topography immediately slopes steeply upwards from the back of the beach, flooding is much less extensive. For such locations, flooding extends just a few meters inland, if there is any flooding at all. The key now is to understand how long populations in each flooded zone have to escape, how quickly the population can escape, and where do they need to go?

4.4 Assessing escape potential

To assess escape potential, we consider the largest (a 30×10^6 m^3 subaerial landslide from position 3) and smallest (a 5×10^6 m^3 submarine landslide from position 9) scenarios considered here (Fig. 6). For subaerial position 3, even for a relatively small volume (5×10^6 m^3) landslide, the inundation area is 19600 m^2 and 489 points are flooded, 372 of which are outside of the threshold time (Fig. 11). For the 30×10^6 m^3, RAEPS located at 20 m asl are flooded, so that the RAEPs have had to be moved upslope to elevations of between 35 and 45 m asl. For this largest scenario, the inundation area is 58000 m^2 and 1450 points are flooded, 1253 of which are outside of the threshold time (Fig. 11).

In the case of submarine position 9, along most of the coastline, only the beaches are inundated, but on the beaches all points are outside of the threshold time. This is a major problem in summer when the island is visited by several thousand tourists each day, who use the beaches to the south and north of the village, the beach zone north of Piscità being the most problematic due to its proximity to the source (Fig. 1). In the village zone, the Punta Lena district (Fig. 1), because of its flat topography, is highly exposed, even in the case of the 5×10^6 m^3 landslide scenario (Fig. 10). The flat topography of the district creates a second problem: the RAEP, which is located at an altitude of 20 m asl, is up to 7-8 minutes away. As a result, all 12 points across Punta Lena are outside of the threshold time, increasing to 82 out of 85 points for the 30×10^6 m^3 case (Fig. 11).

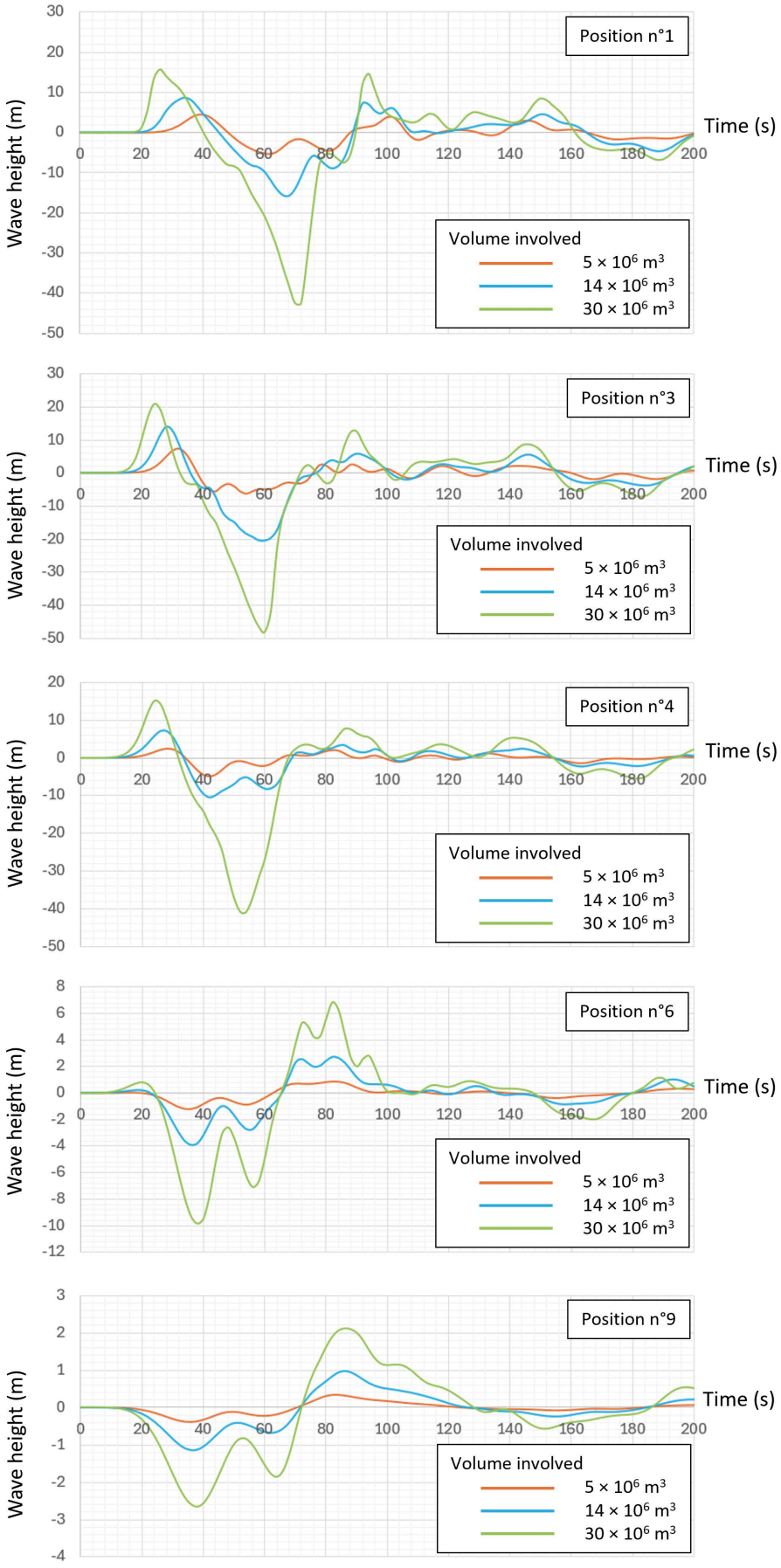

Figure 8. Simulated evolution of wave height with time for 3 volumes and 5 positions at sensor PDC (see text for explanation).

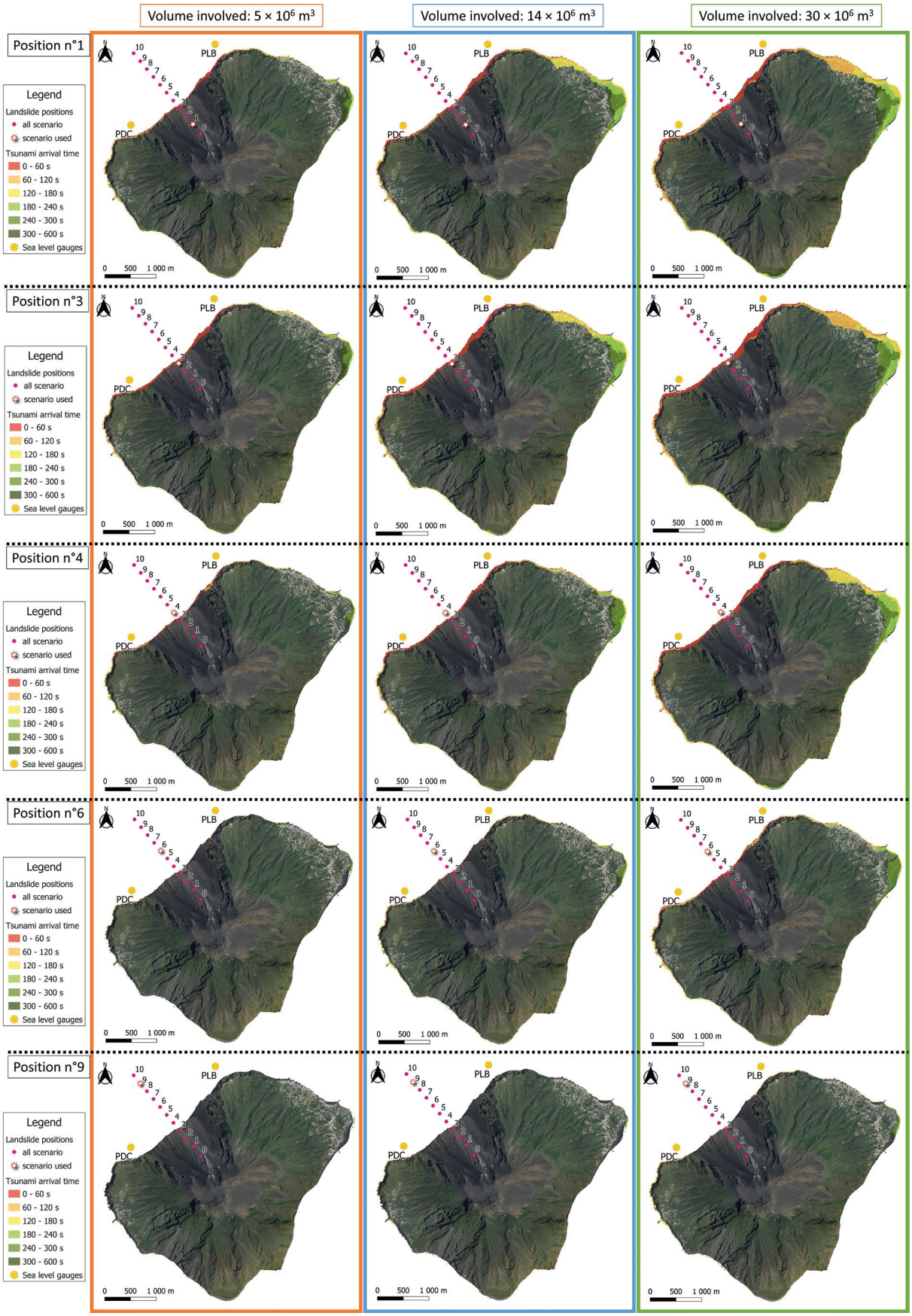

Figure 9. Simulated on tsunami arrival time for three volumes and five positions (see text for explanation).

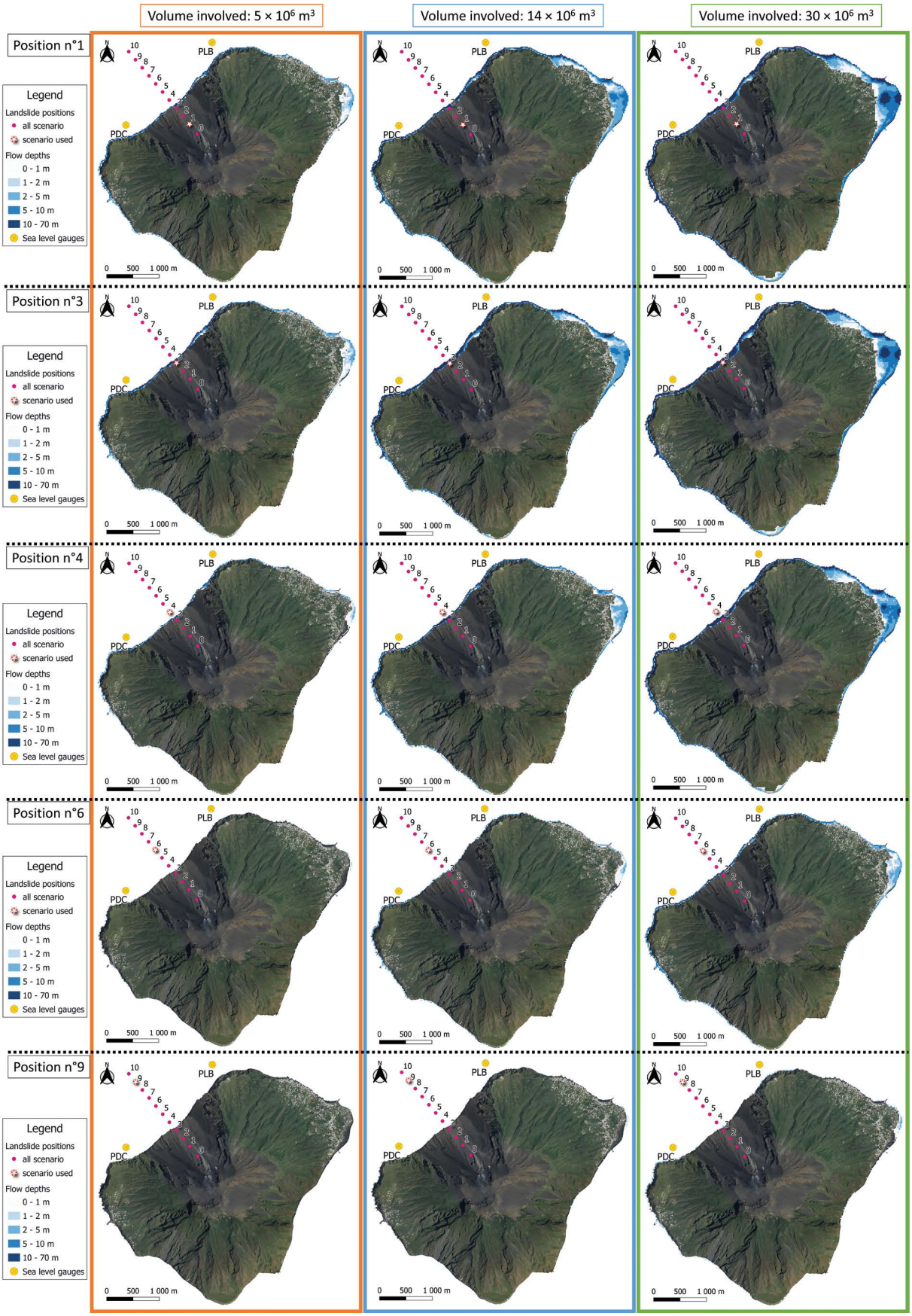

Figure 10. Simulated on land flow depths for three volumes and five positions (see text for explanation).

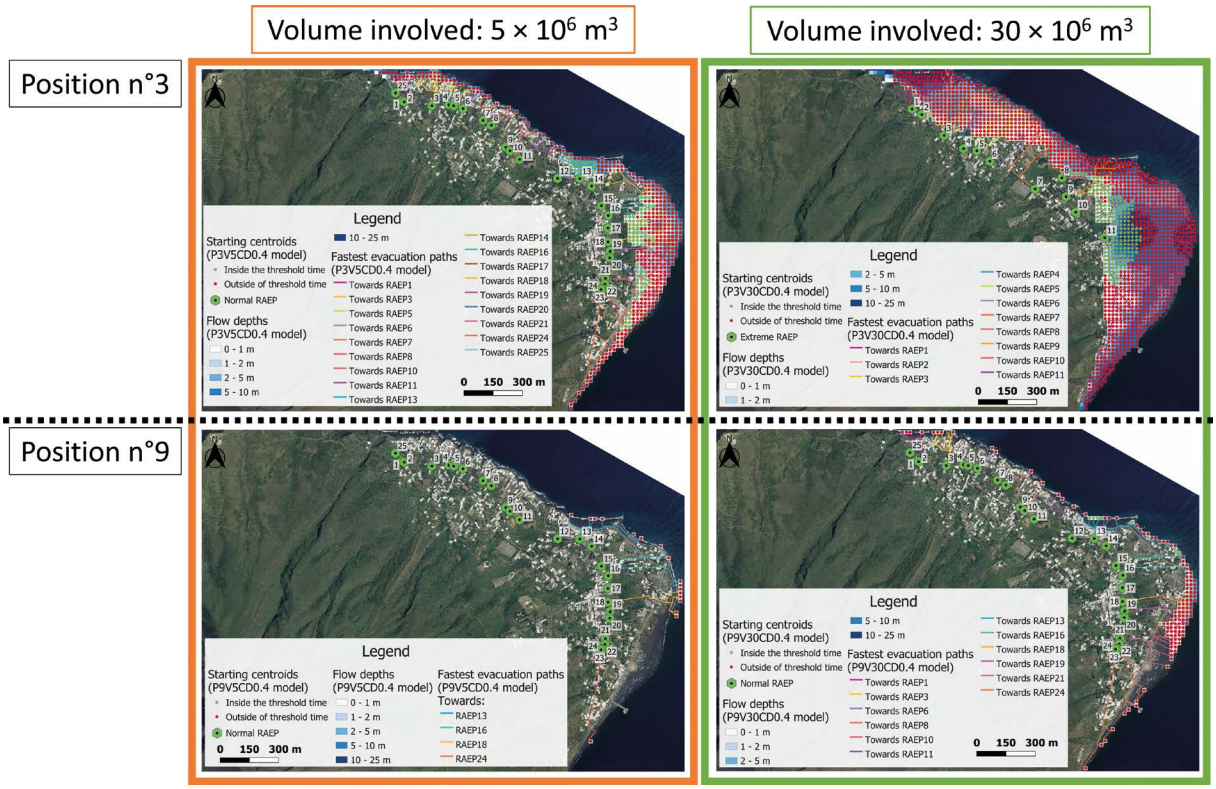

Figure 11. Evacuation plans needed depending on inundation area generated by a tsunami for two landslide volumes (5 and 30 × 10^6 m^3) and positions (Position 3 at a height of 58 m asl and 9 at a depth of −511 m bsl). Two RAEP types are used. The first is at a height of 20 m asl as used by Bonilauri et al. (2021). The second is at a height of 35-45 m asl for extreme scenarios (Bonilauri et al., 2024).

5. Conclusions and perspectives: Towards a protocol for delivery event-tailored tsunami evacuation scenarios prior to wave arrival

Our intention is that the blueprint and protocol developed here can be applied to any case where the exposed population is in the tsunami hazard near-field. The problem with a small island case, as we consider here, is that there is very little time (minutes) before wave arrival, so reaction time needs to be immediate, and the scenarios need to be prepared in advance. However, this is possible using the methodology and alert/assessment system reviewed here (Fig. 12). This approach requires a tight collaboration between research institutions, monitoring agencies and hazard managers, where products need to be suitable for civil protection needs, and thus prepared and communicated under their direction.

The ultimate objective would thus be to deliver escape time assessments before wave arrival in exposed areas. One way to do this would be through the response chain given in Fig. 12. In this chain the first step is to process the pressure sensor signals in real time, using LASSO. LASSO is a statistically based approach which relates the waveform to the passing tsunami to the location of pixels to be inundated. LASSO uses data from the full 156 events considered, thus being valid within the limits of 5-30 × 10^6 m^3 and for landslide positions between 500 m asl and −584 m bsl and allows classification of the event after 40 seconds. This classification then allows the landslide position to be back-located and the wave height to be projected from the library of simulated outcomes. Finally, the inundation extent and assessment of escape time can be delivered. Theoretically, sirens would sound around 24-34 seconds after landslide onset, and the projections would be delivered after 64-74 seconds. Depending on the scenario, especially for pixels in the near-field, alert and projection delivery will be just before wave arrival. However, in the far-field, alert and projection delivery may help with real-time evacuation management. In the former case, the products allow the hazard manager to assess the character of the event immediately. In the latter case, evacuations could be tailored to the case in hand. That is, to avoid congestion, only pixels in need of action could be alerted, and/or RAEPS could be moved up or down slope depending on the degree of inundation. Potential communication means

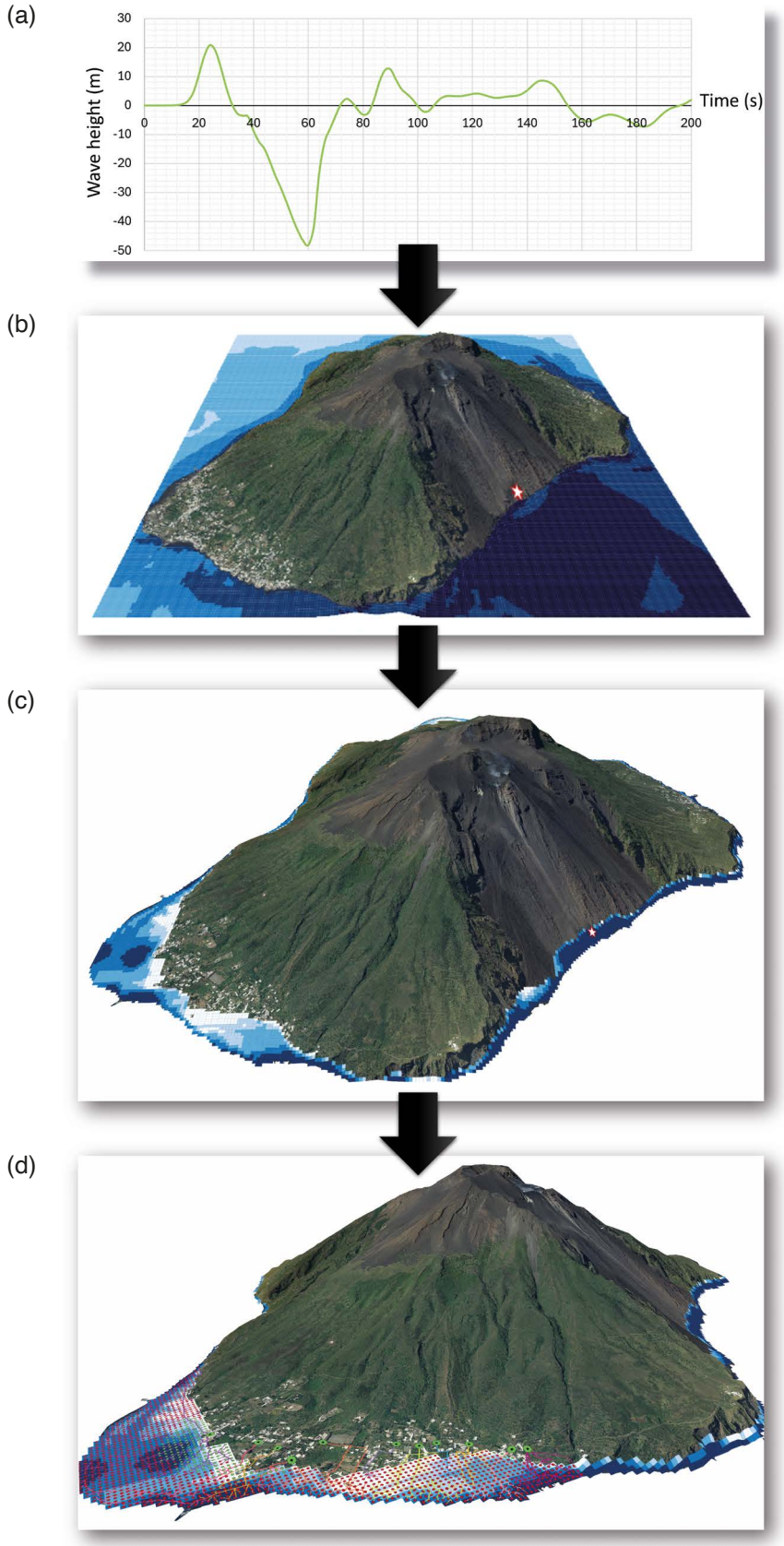

Figure 12. Response example from detection of the landslide tsunami at the sensor to exposure and escape times. (a) Simulated tsunami waveform detected by the pressure sensors. (b) Back projection of landslide source location with generated sea wave height, and (c) forward projection of coastal inundation extent and depth. (d) Pre-prepared evacuation routes and RAEPs for this scenario, with points inside (green) and outside (red) of the threshold time.

could be via cell phone alerts to all devices located in the inundation zone via applications such View Stromboli (https://apps.apple.com/gb/app/view-stromboli/id1551670158).

Data availability statement. All maps produced as part of work of Emmie M. Bonilauri are available on request. Simulation output is available at: https://doi.org/10.13127/stromboli/sciara_del_fuoco_tsunami

Acknowledgements. This work was completed as part of EB's PhD as funded by the French government IDEX-ISITE initiative16 – IDEX-0001 (CAP 20-25), and under the 2023-2024 agreement between Laboratoire Magmas et Volcans (LMV, France) and Istituto Nazionale di Geofisica e Vulcanologia (INGV, Italy). This project was carried out under the 2012-2021 agreement between INGV and the Italian Presidenza del Consiglio dei Ministri, Dipartimento della Protezione Civile (DPC), Convenzione B2, WP2 Task 12 (2019-2021), and through the 2022-2025 agreement between Istituto Nazionale di Geofisica e Vulcanologia (INGV) and DPC (*Convenzione attuativa per lo sviluppo delle attività di servizio*). We thank Eva Delcros for initial figure preparation in QGIS as part of her third year undergraduate (Licence Science de la Terre, Université Clermont Auvergne, L3, 2023-24) internship supported by an InVolc Graduate Track grant. This is contribution no. 667 of the ClerVolc program of the International Research Center for Disaster Sciences and Sustainable Development of the University of Clermont Auvergne.

References

Allen, R. V. (1978). Automatic earthquake recognition and timing from single traces, B. Seismol. Soc. Am., 68, 1521-1532, doi:10.1785/BSSA0680051521.

Bertolaso G., B. De Bernardinis, V. Bosi, C. Cardaci et al. (2009). Civil protection preparedness and response to the 2007 eruptive crisis of Stromboli volcano, Italy, J. Volcanol. Geoth. Res., 182, 3-4, 269-277, doi:10.1016/j.jvolgeores.2009.01.022.

Bonilauri, E. M., A. J. Harris, J. Morin, M. Ripepe et al. (2021). Tsunami evacuation times and routes to safe zones: a GIS-based approach to tsunami evacuation planning on the island of Stromboli, Italy, J. Appl. Volcanol., 10, 4, doi:10.1186/s13617-021-00104-9.

Bonilauri, E. M., C. Aaron, M. Cerminara, R. Paris et al. (2024). Inundation and evacuation of shoreline populations during landslide-triggered tsunamis: An integrated numerical and statistical hazard assessment. Natural Hazards and Earth System Sciences, 24, 11, 3789-3813, doi:10.5194/nhess-24-3789-2024.

Calvari, S. and G. Groppelli (1996). Relevance of the Chiancone volcaniclastic deposit in the recent history of Etna Volcano (Italy), J. Volcanol. Geoth. Res., 72, 3-4, 239-258, doi:10.1016/0377-0273(96)00012-1.

Carvajal, M., C. Araya-Cornejo, I. Sepúlveda, D. Melnick et al. (2019). Nearly instantaneous tsunamis following the Mw 7.5 2018 Palu earthquake, Geophys. Res. Lett., 46, 10, 5117-5126, doi:10.1029/2019GL082578.

Cerminara, M., T. Esposti Ongaro, M. De' Michieli Vitturi, A. Tadini et al. (2024). Simulated scenarios of volcanic mass movements and associated tsunamis at Stromboli (Aeolian archipelago, Tyrrhenian Sea, Italy), version 1 [Data set]. Istituto Nazionale di Geofisica e Vulcanologia (INGV), doi:10.13127/stromboli/sciara_del_fuoco_tsunami.

Chacón-Barrantes, S., F. Rivera-Cerdas and A. Murillo-Gutiérrez (2023). Impact of the tsunami caused by the Hunga Tonga-Hunga Ha'apai eruption in Costa Rica on 15 January 2022, B. Volcanol., 85, 36, doi:10.1007/s00445-023-01648-x.

Chiocci, F., C. Romagnoli, P. Tommasi and A. Bosman (2008) The Stromboli 2002 tsunamigenic submarine slide: characteristics and possible failure mechanisms, J. Geophys. Res., 113, doi:10.1029/2007JB005172(B10).

Denlinger, R. P. and J. K. Morgan (2014). Instability of Hawaiian volcanoes. Characteristics of Hawaiian volcanoes, in M. P. Poland, T. J. Takahashi and C. M. Landowski (Editors), U. S. Geological Survey Professional Paper 1801, 149-176, doi:10.3133/pp18014.

Dudley, W. C. (1998). Tsunami!, University of Hawaii Press, Honolulu, 362.

Eaton, J. P., D. H. Richter and W. U. Ault (1961). The tsunami of May 23, 1960, on the Island of Hawaii, B. Seismol. Soc. Am., 51, 2, 135-157, doi:10.1785/BSSA0510020135.

Esposti Ongaro, T., M. de' Michieli Vitturi, M. Cerminara, A. Fornaciai et al. (2021). Modeling tsunamis generated by submarine landslides at Stromboli Volcano (Aeolian Islands, Italy): A numerical benchmark study, Front. Earth Sci., 9, doi:10.3389/feart.2021.628652.

Felton, E. A., K. A. Crook and B. H. Keating (2000). The Hulopoe gravel, Lanai, Hawaii: new sedimentological data and their bearing on the "giant wave" (mega-tsunami) emplacement hypothesis, Pure Appl. Geophys., 157, 1257-1284, doi:10.1007/s000240050025.

Fernández-Nieto, E., M. Parisot, Y. Penel and J. Sainte-Marie (2018). A hierarchy of dispersive layer-averaged approximations of Euler equations for free surface flows, Commun. Math. Sci., 16, 1169-1202, doi:10.4310/CMS.2018.v16.n5.a01.

Fornaciai, A., M. Favalli and L. Nannipieri (2019). Numerical simulation of the tsunamis generated by the Sciara del Fuoco landslides (Stromboli Island, Italy), Sci. Rep., 9, 18542, doi:10.1038/s41598-019-54949-7.

Giordano, G. and G. De Astis (2021). The summer 2019 basaltic Vulcanian eruptions (paroxysms) of Stromboli, B. Volcanol., 83, 1, doi:10.1007/s00445-020-01423-2.

Grilli, S. T., D. R. Tappin, S. Carey, S. F. Watt et al. (2019). Modelling of the tsunami from the December 22, 2018 lateral collapse of Anak Krakatau volcano in the Sunda Straits, Indonesia, Sci. Rep., 9, 11946, doi:10.1038/s41598-019-48327-6.

Helsley, B. K. and C. E. Helsley (2012). Traces of coral bearing deposits on Lanai, Hawaii, and implications for their origin (island uplift vs. giant tsunami), in Gloria I. Lopez (Editor), Tsunami-Analysis of a Hazard-From Physical Interpretation to Human Impact, IntechOpen, 270, ISBN 978-953-51-0865-8, doi:10.5772/50875.

Johnson, C. and C. L. Mader (1994). Modeling the 105 ka Lanai tsunami, Sci. Tsunami Hazards, 12, 33-38.

Klettner, C., S. Balasubramanian, J. Hunt, H. Fernando et al. (2012). Draw-down and run-up of tsunami waves on sloping beaches, Proceedings of the Institution of Civil Engineers-Engineering and Computational Mechanics, 165, 2, 119-129, doi:10.1680/eacm.10.00044.

Kokelaar, P. and C. Romagnoli (1995). Sector collapse, sedimentation and clast population evolution at an active island-arc volcano: Stromboli, Italy. B. Volcanol., 57,4, 240-262, doi:10.1007/BF00265424.

Lodato, L., L. Spampinato, A. Harris, S. Calvari et al. (2007). The morphology and evolution of the Stromboli 2002-2003 lava flow field: an example of a basaltic flow field emplaced on a steep slope, B. Volcanol., 69, 661-679, doi:10.1007/s00445-006-0101-6.

Lynett, P., M. McCann, Z. Zhou, W. Renteria et al. (2022). Diverse tsunamigenesis triggered by the Hunga Tonga-Hunga Ha'apai eruption, Nature, 609, 7928, 728-733, doi:10.1038/s41586-022-05170-6.

Mader, C. L. (2001). Modeling the La Palma landslide tsunami, Sci. Tsunami Hazards, 19, 3, 150-170.

Maramai, A., L. Graziani, G. Alessio, P. Burrato et al. (2005). Near-and far-field survey report of the 30 December 2002 Stromboli (southern Italy) tsunami, Mar. Geol., 215,1-2, 93-106, doi:10.1016/j.margeo.2004.11.009.

Macías, J., C. Escalante and M. J. Castro, (2021). Multilayer-HySEA model validation for landslide-generated tsunamis – Part 1: Rigid slides, Nat. Hazard Earth Sys., 21, 775-789, doi:10.5194/nhess-21-775-2021.

Macías, J., C. Escalante and M. J. Castro (2021b). Multilayer-HySEA model validation for landslide-generated tsunamis – Part 2: Granular slides, Nat. Hazard Earth Sys., 21, 791-805, doi:10.5194/nhess-21-791-2021.

Mattox, T. N. and M. T. Mangan (1997). Littoral hydrovolcanic explosions: a case study of lava-seawater interaction at Kilauea Volcano, J. Volcanol. Geoth. Res., 75, 1-2, 1-17.

McMurtry, G. M., G. J. Fryer, D. R. Tappin, I. P. Wilkinson et al. (2004). Megatsunami deposits on Kohala volcano, Hawaii, from flank collapse of Mauna Loa, Geology, 32, 9, 741-744, doi:10.1130/G20642.1.

Moore, A. L. (2000). Landward fining in onshore gravel as evidence for a late Pleistocene tsunami on Molokai, Hawaii, Geology, 28, 3, 247-250, doi:10.1130/0091-7613(2000)28<247:LFIOGA>2.0.CO;2.

Mutaqin, B. W., F. Lavigne, D. S. Hadmoko and M. N. Ngalawan (2019, April). Volcanic eruption-induced tsunami in Indonesia: A review, in IOP Conference Series, Earth Environ. Sci., 256, 1, 012023, IOP Publishing, doi:10.1088/1755-1315/256/1/012023.

Normark, W. R., J. G. Moore and M. E. Torresan (1993). Giant volcano-related landslides and the development of the Hawaiian Islands, in Submarine landslides: selected studies in the US Exclusive Economic Zone, 2002, Bull. U. S. Geol. Surv., Denver, 184-196.

Pararas-Carayannis, G. (2002). Evaluation of the threat of mega tsunami generation from postulated massive slope failures of island stratovolcanoes on La Palma, Canary Islands and on the island of Hawaii, Sci. Tsunami Haz., 20, 5, 251-277.

Pareschi, M. T., E. Boschi and M. Favalli, (2006). Lost tsunami, Geophys. Res. Let., 33, 22, doi:10.1029/2006GL027790.

Pareschi, M. T., E. Boschi and M. Favalli (2007). Holocene tsunamis from Mount Etna and the fate of Israeli Neolithic communities, Geophys. Res. Lett., 34, 16, doi:10.1029/2007GL030717.

Paris, A., P. Heinrich, R. Paris and S. Abadie (2020). The December 22, 2018 Anak Krakatau, Indonesia, landslide and tsunami: preliminary modeling results, Pure Appl. Geophys., 177, 2, 571-590, doi:10.1007/s00024-019-02394-yf.

Paris, R. (2015). Source mechanisms of volcanic tsunamis, Phil. Trans. R. Soc., A.37320140380, doi:10.1098/rsta.2014.0380.

Paris, R., A. D. Switzer, M. Belousova A. Belousov et al. (2014a). Volcanic tsunami: A review of source mechanisms, past events, and hazards in Southeast Asia (Indonesia, Philippines, Papua New Guinea), Nat. Hazards, 70, 1, 447-470, doi:10.1007/s11069-013-0822-8.

Paris, R., P. Wassmer, F. Lavigne, A. Belousov et al. (2014b). Coupling eruption and tsunami records: The Krakatau 1883 case-study, Indonesia, B. Volcanol., 76, 814, doi:10.1007/s00445-014-0814-x.

Pistolesi, M., A. Bertagnini, A. Di Roberto, M. Ripepe et al. (2020). Tsunami and tephra deposits record interactions between past eruptive activity and landslides at Stromboli volcano, Italy, Geology, 48, 5, 436-440, doi:10.1130/G47331.1.

Ripepe, M. and G. Lacanna (2024). Volcano generated tsunami recorded in the near source, Nat. Commun., 15, 1, 1802, doi:10.1038/s41467-024-45937-1.

Roberto, A., A. Bertagnini, M. Pompilio and M. Bisson (2014). Pyroclastic density currents at Stromboli volcano (Aeolian Islands, Italy): a case study of the 1930 eruption, Bull. Volcanol., 76, doi:10.1007/s00445-014-0827-5(6).

Röbke, B. R. and A. Vött (2017). The tsunami phenomenon, Progr. Oceanogr., 159, 296-322, doi:10.1016/j.pocean.2017.09.003.

Rosi, M., S. T. Levi, M. Pistolesi, A. Bertagnini et al. (2019). Geoarchaeological evidence of middle-age tsunamis at Stromboli and consequences for the tsunami hazard in the Southern Tyrrhenian Sea, Sci. Reports, 9, 1, 1-10, doi:10.1038/s41598-018-37050-3.

Schindelé, F., L. Kong, E. M. Lane, R. Paris et al. (2024). A Review of Tsunamis Generated by Volcanoes (TGV) Source Mechanism, Modelling, Monitoring and Warning Systems, Pure Appl. Geophys., 1-48, doi:10.1007/s00024-024-03515-y.

Simkin, T. and R. S. Fiske (1983). Krakatau 1883: The volcanic eruption and its effects, Smithsonian Institution Press, Washington DC, 464, doi:10.1002/esp.3290100118.

Smith, J. R., K. Satake, J. K. Morgan and P. W. Lipman (2002). Submarine landslides and volcanic features on Kohala and Mauna Kea volcanoes and the Hana Ridge, Hawaii, Hawaiian volcanoes: Deep underwater perspectives, 128, 11-28, Eiichi Takahashi, Peter W. Lipman, Michael O. Garcia, Jiro Naka, Shigeo Aramaki (Editors), doi:10.1029/GM128p0011.

Stearns, H. T. (1938). Ancient Shorelines on the Island of Lanai, Hawaii, Geolog. Soc. Am. Bull. 49, 615-628, doi:10.1130/gsab-49-615.

Tehranirad, B., J. C. Harris, A. R. Grilli, S. T. Grilli et al. (2015). Far-field tsunami impact in the North Atlantic basin from large scale flank collapses of the Cumbre Vieja Volcano, La Palma, Pure Appl. Geophys., 172, 3589-3616, ff10.1007/s00024-015-1135-5f.

Tibaldi, A. (2001). Multiple sector collapses at stromboli volcano, Italy: how they work, Bull. Volcanol. 63, 2-3,112-125, doi:10.1007/s004450100129.

Tibshirani, R. (1996). Regression shrinkage and selection via the lasso, J. R. Stat. Soc., Series B, 58, 1, 1996, 267-288, http://www.jstor.org/stable/2346178.

Tinti, S., E. Bortolucci and C. Romagnoli (2000). Computer simulations of tsunamis due to sector collapse at Stromboli, Italy., J. Volcanol. Geoth. Res., 96, 1-2, 103-128, doi:10.1016/S0377-0273(99)00138-9.

Tinti, S., G. Pagnoni and F. Zaniboni (2006a). The landslides and tsunamis of the 30th of December 2002 in Stromboli analysed through numerical simulations, Bull. Volcanol., 68, 5, 462-479, doi:10.1007/s00445-005-0022-9.

Tinti, S., A. Maramai, A. Armigliato, L. Graziani et al. (2006b). Observations of physical effects from tsunamis of December 30, 2002 at Stromboli volcano, southern Italy, Bull. Volcanol., 68, 5, 450-461, doi:10.1007/s00445-005-0021-x.

Ward, S. N. and S. Day (2001). Cumbre Vieja volcano-potential collapse and tsunami at La Palma, Canary Islands, Geophys. Res. Lett., 28, 17, 3397-3400, doi:10.1029/2001GL013110.

***CORRESPONDING AUTHOR: Andrew HARRIS**,
Université Clermont Auvergne, Laboratoire Magmas et Volcans, Aubière, France
e-mail: andrew.harris@uca.fr